Modal Analysis of a Two-Parachute System

Jing Pei[*], Carlos M. Roithmayr[†]

NASA Langley Research Center, Hampton, Virginia, 23681

Richard L. Barton[‡] and Daniel A. Matz[§]

NASA Johnson Space Center, Houston, Texas, 77058

   The Orion capsule is designed to land under a nominal configuration of three main parachutes; however, the system is required to be fault tolerant and land successfully if one of the main parachutes fails to open. The Capsule Parachute Assembly System (CPAS) Team performed a series of drop tests in order to characterize the performance of the system with two main parachutes. During the series of drop tests, several distinct dynamical modes were observed. The most consequential of these is the pendulum mode. Three other modes are benign: flyout (scissors), maypole, and breathing. The actual multi-body system is nonlinear, flexible, and possesses significant cross-coupling. Rather than perform analysis of this highly complex system directly, we conduct analysis of each dynamical mode observed during flight, based on first principles. This approach is analogous to traditional aircraft flight dynamics analysis in which the full nonlinear behavior of the airframe is decomposed into longitudinal dynamics (phugoid and short-period modes) and lateral dynamics (spiral, roll-subsidence, and dutch-roll modes). This analysis is intended to supplement multi-body nonlinear simulations in order to provide further insight into the system.

I.   Introduction

   As discussed in Refs. [1] and [2], a series of flight tests was conducted to characterize the performance of the Orion Multi Purpose Crew Vehicle (MPCV) parachute cluster. It is apparent from flight tests that the system made up of two main parachutes and a capsule can undergo several distinct dynamical behaviors. The most significant and problematic of these is the pendulum mode in which the system develops a pronounced swinging motion with amplitude of up to 24 deg. Large excursions away from vertical by the capsule could cause it to strike the ground at a large horizontal or vertical speed and jeopardize the safety of the astronauts during a crewed mission. In Ref. [2] Ali et al. summarized a series of efforts taken by the CPAS program to understand and mitigate the pendulum issue. Other noticeable but benign modes include: 1) flyout (scissors) mode, where the parachutes move back and forth symmetrically with respect to the vertical axis, similar to the motion of a pair of scissors, 2) maypole mode, where the two parachutes circle around the vertical axis at a nearly constant radius and period, and 3) breathing mode, in which deformation of the non-rigid canopies affects the axial acceleration of the system in an oscillatory fashion. Because these modes are relatively harmless, little effort has been devoted to analyzing them compared to the pendulum motion.

   Over the past 50 years, a number of analytical, numerical, and experimental investigations have been performed with the goal of understanding parachute-payload system pitch-plane dynamics and pendulum motion (for example, Refs. [3]–[6]). Reference [7] used Computational Fluid Dynamics (CFD) to study the stability of various main parachute configurations from the Apollo and MPCV programs. It was demonstrated that an increase in the porosity of the parachute improved its stability characteristics and hence reduced the

---

[*]Aerospace Engineer, Vehicle Analysis Branch
[†]Senior Aerospace Engineer, Vehicle Analysis Branch
[‡]Branch Chief, Aeroscience Branch (retired)
[§]Aerospace Engineer, Flight Mechanics and Trajectory Design Branch

American Institute of Aeronautics and Astronautics

severity of the pendulum motion. Reference [6] provides similar insights regarding the flow physics associated with non-porous vs. porous configurations and how it affects the parachute stability characteristics. Most recently, Refs. [8] and [9] provide further analytical investigation of the two-parachute cluster pendulum motion via linear and non-linear analyses. Figure 1 shows a typical C_N vs. α profile for an unstable parachute such as the MPCV main parachute. The aerodynamic normal force for each parachute is a nonlinear function of angle of attack, α, with two stable equilibrium points at $\pm\alpha_0$.[3,6,7] The effect of the C_N profile on the pendulum motion is well studied. The effect of C_N on the characteristics of the other modes will be examined as a part of this work.
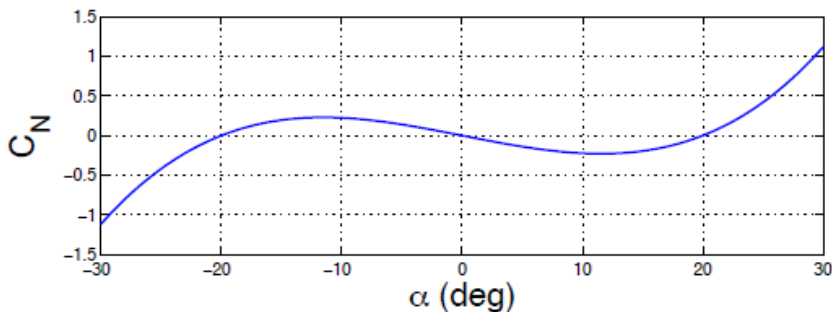

Figure 1. C_N **vs.** α **curve for unstable parachutes**

Motions of the actual system made up of two parachutes and a capsule are extremely complicated due to nonlinearities and flexibility effects. Often it is difficult to obtain insight into the fundamental dynamics of the system by examining results from a multi-body simulation based on nonlinear equations of motion.[?,?] In the current work, the dynamics of each mode observed during flight is derived from first principles on an individual basis by making numerous simplifications along the way. The intent is to gain a better understanding into the behavior of the complex multi-body system by studying the reduced set of differential equations associated with each mode. This approach is analogous to the traditional modal analysis technique used to study airplane flight dynamics[11] in which the full nonlinear behavior of the airframe is decomposed into the phugoid and short period modes for the longitudinal dynamics, and the spiral, roll-subsidence, and dutch-roll modes for the lateral dynamics. The current paper takes the same analytical approach as Ref. [8] and [9] for the pendulum mode but focuses on the other three dynamical modes of the two-parachute configuration. The pendulum mode is discussed briefly for completeness. It is important to note that the paper does not address the mechanisms that cause the system to transition from one mode to another, nor does it discuss motions during which two or more modes occur simultaneously. According to Ref. [12], it is not obvious that there is always a unique stable configuration for a cluster of unstable parachutes. The remainder of the paper is organized as follows. Section II briefly addresses the pendulum mode along with the C_N vs. α model identified from flight test data.[9] A simplified planar model of the scissors mode is presented in Sec. III. Section IV analyzes the maypole motion and provides insights based on flight data regarding how aerodynamics can affect the characteristics of the maypole motion. "Breathing" motion of non-rigid parachutes is studied in Sec. V. Conclusions are presented in Sec. VI. **Note: Due to ITAR (International Tariff and Arms Regulation) restrictions, all aerodynamic parameters shown in this paper are placeholders. Y-axis labels have been removed for figures with flight data.**

II.   Pendulum Mode

Results from contemporary studies of the pendulum motion are reviewed briefly; details of the analyses can be found in Refs. [8] and [9]. The planar dumbbell model used to study the underlying dynamics of the pendulum motion is illustrated in Fig. 2. The capsule is modeled as a particle rather than an extended rigid body and aerodynamic forces acting on the capsule are ignored.[3] The two parachutes are treated as a single particle. The rigid body B contains two particles. Particle P_C has a mass of m_C, the total mass of two parachutes, which includes dry mass as well as the mass of air trapped in each of the canopies. Particle P_L has a mass of m_L and represents the capsule. Body B moves such that P_C and P_L remain at all times in

a plane fixed in a Newtonian reference frame N. A right-handed set of mutually perpendicular unit vectors $\hat{\mathbf{n}}_1$, $\hat{\mathbf{n}}_2$, and $\hat{\mathbf{n}}_3$ is fixed in N. Unit vectors $\hat{\mathbf{n}}_1$ and $\hat{\mathbf{n}}_3$ lie in the plane in which motion takes place, and are directed as shown in Fig. 2; $\hat{\mathbf{n}}_1$ is horizontal, $\hat{\mathbf{n}}_2$ is directed into the page, and $\hat{\mathbf{n}}_3$ is vertical, directed downward. A right-handed set of mutually perpendicular unit vectors $\hat{\mathbf{b}}_1$, $\hat{\mathbf{b}}_2$, and $\hat{\mathbf{b}}_3$ is fixed in B. Unit vectors $\hat{\mathbf{b}}_1$ and $\hat{\mathbf{b}}_3$ are directed as shown in Fig. 2; $\hat{\mathbf{b}}_1$ has the same direction as the position vector $\mathbf{r}^{P_C P_L}$ from P_C to P_L. Unit vector $\hat{\mathbf{b}}_2$ is directed into the page; note that it is fixed in N as well as in B.
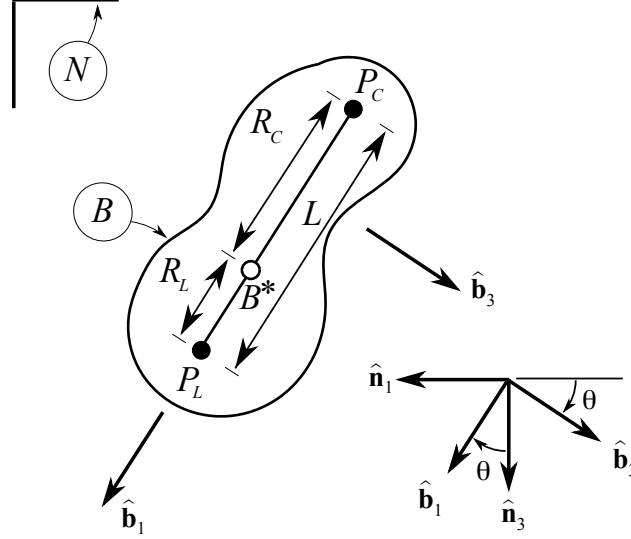

Figure 2. Rigid Body Containing Two Particles.

The following two relationships governing translation and rotation of the dumbbell are derived in Ref. [8].

$$^N \mathbf{a}^{B^\star} = \frac{1}{m_C + m_L}\left\{ -\left[A_x \sin\theta + A_z \cos\theta\right]\hat{\mathbf{n}}_1 + \left[W_C + W_L - A_x \cos\theta + A_z \sin\theta\right]\hat{\mathbf{n}}_3\right\} \quad (1)$$

$$\ddot{\theta} + \frac{1}{m_C L}\left[(m_C\, g - W_C)\sin\theta - A_z\right] = 0 \quad (2)$$

where $W_L = m_L\, g$, and g is the magnitude of the local gravitational force per unit of mass. W_C is the sum of dry weights of the two parachutes; the weight of the air trapped in their canopies is ignored because the gravitational force exerted on that air is assumed to be counteracted by buoyancy effects from the ambient atmosphere. A_x, the magnitude of the resultant of the aerodynamic axial forces applied to the two parachutes, can be expressed as:

$$A_x = 2q_\infty S_{\mathrm{ref}} C_A \quad (3)$$

where q_∞ is the dynamic pressure, S_{ref} is the reference area of a single parachute, and C_A is the drag coefficient for a single parachute. The absolute value of A_z is the magnitude of the resultant of the aerodynamic normal forces applied to the two parachutes; A_z can be expressed as:

$$A_z = -2q_\infty S_{\mathrm{ref}} C_N \quad (4)$$

C_N is the aerodynamic normal force coefficient for a single parachute. As discussed in Ref. [3] and [4], C_A and C_N are nonlinear functions of α, the instantaneous angle of attack of the parachute:

$$C_A = C_{A_o} + \frac{1}{2}C_{A_\alpha}\alpha_0\left(\frac{\alpha^2}{\alpha_0{}^2} - 1\right) \quad (5)$$

$$C_N(\alpha) = \frac{C_{N_\alpha}}{2\alpha_0^2}\left(\alpha^3 - \alpha_0{}^2\alpha\right) \quad (6)$$

Here α_0 is the stable trim angle of attack and C_{N_α} is the slope of the C_N curve at α_0. An additional damping term, $C_{N_{\dot{\alpha}}}$, was added to Eqs. (6) to account for unsteady time lag effects in the rotational degree-of-freedom.[8,9,13] Table 1 shows the parameter estimation results[9] from applying the output-error method in

American Institute of Aeronautics and Astronautics

system identification theory[14,15] based on the pendulum motion observed from CDT (Capsule Drop Test) 3-11 and 3-12 flights. The estimated parameters and the their standard errors are listed in columns 2 and 3, respectively.

Table 1. Parameter Estimation Results from CDT 3-11

parameter	$\hat{\theta}$	$s(\hat{\theta})$
α_0 (rad)	0.23	0.1
C_{N_α} (rad^{-1})	0.4	0.1
$C_{N_{\dot{\alpha}}}$ (rad/s)$^{-1}$	1.5	0.3

III. Scissors Mode

Ref. [1] describes the flyout or scissors motion as two parachutes moving sinusoidally away from or towards the vertical axis in a symmetrical fashion, while the capsule descends at nearly constant speed. A simple planar model involving three particles is used to study the underlying dynamics of the scissors motion as shown in Fig. 3. Particle P_L has a mass of m_L and represents the capsule. The two parachutes are treated as identical particles, P_B and P_C; each has a mass of m_C, which includes dry mass as well as the mass of air trapped inside the canopy. The system moves such that the three particles remain at all times in a plane fixed in a Newtonian reference frame N. A right-handed set of mutually perpendicular unit vectors $\hat{\mathbf{n}}_1$, $\hat{\mathbf{n}}_2$, and $\hat{\mathbf{n}}_3$ is fixed in N. Unit vectors $\hat{\mathbf{n}}_1$ and $\hat{\mathbf{n}}_3$ lie in the plane in which motion takes place, and are directed as shown in Fig. 3; $\hat{\mathbf{n}}_1$ is horizontal, $\hat{\mathbf{n}}_2$ is directed out of the page, and $\hat{\mathbf{n}}_3$ is vertical, directed downward. P_B and P_C each are connected to P_L by a massless, rigid link; the two links are connected by a revolute joint whose axis is parallel to $\hat{\mathbf{n}}_2$. P_B and one link are fixed in a reference frame B, whereas P_C and the other link are fixed in a reference frame C. The orientations of B and C in N are described by angles θ_1 and θ_2, respectively. A dextral set of mutually perpendicular unit vectors $\hat{\mathbf{b}}_1$, $\hat{\mathbf{b}}_2$, and $\hat{\mathbf{b}}_3$ is fixed in B and directed as shown in Fig. 3; $\hat{\mathbf{b}}_2$ is directed out of the page. A similar set of unit vectors $\hat{\mathbf{c}}_1$, $\hat{\mathbf{c}}_2$, and $\hat{\mathbf{c}}_3$ is fixed in C; $\hat{\mathbf{c}}_2$ is directed into the page. The relationships of each set of unit vectors to $\hat{\mathbf{n}}_1$, $\hat{\mathbf{n}}_2$, and $\hat{\mathbf{n}}_3$ are given in Tables 2 and 3, respectively. For example, the entry in the rth row and sth column (not counting the row or the column containing unit vectors) of Table 2 is the dot product $\hat{\mathbf{n}}_r \cdot \hat{\mathbf{b}}_s$ $(r, s = 1, 2, 3)$. Note that $\hat{\mathbf{b}}_2$ and $\hat{\mathbf{c}}_2$ are each fixed in the three reference frames N, B, and C. The resultant external forces acting on P_L, P_B, and P_C are denoted by $\mathbf{F}_L$, $\mathbf{F}_B$, and $\mathbf{F}_C$, respectively.

The equation of motion governing the horizontal speed of P_L, which is not presented, shows that horizontal acceleration of P_L vanishes under the following conditions: $(\mathbf{F}_L + \mathbf{F}_B + \mathbf{F}_C) \cdot \hat{\mathbf{n}}_1 = 0$, $\theta_1 = \theta_2$, $\dot{\theta}_1 = \dot{\theta}_2$, and $\ddot{\theta}_1 = \ddot{\theta}_2$. The latter three conditions simply correspond to the symmetric motion of the parachutes that characterizes the scissors behavior under consideration. In what follows we assume all four conditions exist, and take the horizontal speed of P_L to be constant and equal to zero. In that case, the three-particle system has three degrees of freedom in N, and three motion variables u_1, u_2, and u_3 are introduced operationally as follows. The velocity $^N\mathbf{v}^{P_L}$ of P_L in N is given by

$$^N\mathbf{v}^{P_L} = w_L\hat{\mathbf{n}}_3 = u_1\hat{\mathbf{n}}_3 \tag{7}$$

The angular velocities in N of B and C are, respectively

$$^N\boldsymbol{\omega}^B = -\dot{\theta}_1\hat{\mathbf{b}}_2 = -u_2\hat{\mathbf{b}}_2 \tag{8}$$

$$^N\boldsymbol{\omega}^C = -\dot{\theta}_2\hat{\mathbf{c}}_2 = -u_3\hat{\mathbf{c}}_2 \tag{9}$$

After noting that P_L is fixed in B and also in C, the velocities in N of P_B and P_C can be expressed as

$$^N\mathbf{v}^{P_B} = {}^N\mathbf{v}^{P_L} + {}^N\boldsymbol{\omega}^B \times (-L\hat{\mathbf{b}}_3) = u_1\hat{\mathbf{n}}_3 + Lu_2\hat{\mathbf{b}}_1 \tag{10}$$

$$^N\mathbf{v}^{P_C} = {}^N\mathbf{v}^{P_L} + {}^N\boldsymbol{\omega}^C \times (-L\hat{\mathbf{c}}_3) = u_1\hat{\mathbf{n}}_3 + Lu_3\hat{\mathbf{c}}_1 \tag{11}$$
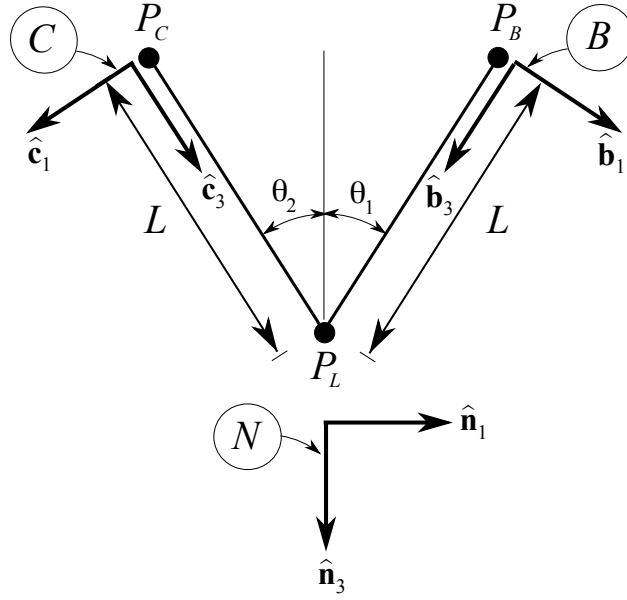
American Institute of Aeronautics and Astronautics

Figure 3. Scissors Mode Planar Model

<table>
<tr><th>Table 2. Direction Cosines, $\hat{\mathbf{n}}_r \cdot \hat{\mathbf{b}}_s$.</th></tr>
</table>

	$\hat{\mathbf{b}}_1$	$\hat{\mathbf{b}}_2$	$\hat{\mathbf{b}}_3$
$\hat{\mathbf{n}}_1$	$\cos\theta_1$	0	$-\sin\theta_1$
$\hat{\mathbf{n}}_2$	0	1	0
$\hat{\mathbf{n}}_3$	$\sin\theta_1$	0	$\cos\theta_1$

Table 3. Direction Cosines, $\hat{\mathbf{n}}_r \cdot \hat{\mathbf{c}}_s$.

	$\hat{\mathbf{c}}_1$	$\hat{\mathbf{c}}_2$	$\hat{\mathbf{c}}_3$
$\hat{\mathbf{n}}_1$	$-\cos\theta_2$	0	$\sin\theta_2$
$\hat{\mathbf{n}}_2$	0	-1	0
$\hat{\mathbf{n}}_3$	$\sin\theta_2$	0	$\cos\theta_2$

Kane's partial velocities[16] ${}^N\mathbf{v}_r^{P_L}$, ${}^N\mathbf{v}_r^{P_B}$, and ${}^N\mathbf{v}_r^{P_C}$ are obtained by inspecting the expressions for ${}^N\mathbf{v}^{P_L}$, ${}^N\mathbf{v}^{P_B}$, and ${}^N\mathbf{v}^{P_C}$ for the vector coefficients of the motion variables u_r $(r = 1, 2, 3)$. The partial velocities are recorded in Table 4.

Table 4. Partial Velocities, Scissors Motion

r	${}^N\mathbf{v}_r^{P_L}$	${}^N\mathbf{v}_r^{P_B}$	${}^N\mathbf{v}_r^{P_C}$
1	$\hat{\mathbf{n}}_3$	$\hat{\mathbf{n}}_3$	$\hat{\mathbf{n}}_3$
2	$\mathbf{0}$	$L\hat{\mathbf{b}}_1$	$\mathbf{0}$
3	$\mathbf{0}$	$\mathbf{0}$	$L\hat{\mathbf{c}}_1$

The acceleration ${}^N\mathbf{a}^{P_L}$ of P_L is given by

$$ {}^N\mathbf{a}^{P_L} = \dot{u}_1\hat{\mathbf{n}}_3 \tag{12} $$

The angular accelerations in N of B and C are simply

$$ {}^N\boldsymbol{\alpha}^B = -\dot{u}_2\hat{\mathbf{b}}_2 \tag{13} $$

$$ {}^N\boldsymbol{\alpha}^C = -\dot{u}_3\hat{\mathbf{c}}_2 \tag{14} $$

Keeping in mind that P_L is fixed in B and also in C, the accelerations in N of P_B and P_C are given by

$$ {}^N\mathbf{a}^{P_B} = {}^N\mathbf{a}^{P_L} + {}^N\boldsymbol{\alpha}^B \times (-L\hat{\mathbf{b}}_3) + {}^N\boldsymbol{\omega}^B \times {}^N\boldsymbol{\omega}^B \times (-L\hat{\mathbf{b}}_3) = \dot{u}_1\hat{\mathbf{n}}_3 + \dot{u}_2\hat{\mathbf{b}}_2 \times L\hat{\mathbf{b}}_3 - u_2\hat{\mathbf{b}}_2 \times Lu_2\hat{\mathbf{b}}_1 $$

$$ = \dot{u}_1\hat{\mathbf{n}}_3 + L(\dot{u}_2\hat{\mathbf{b}}_1 + u_2{}^2\hat{\mathbf{b}}_3) \tag{15} $$

American Institute of Aeronautics and Astronautics

$$^N\mathbf{a}^{P_C} = {}^N\mathbf{a}^{P_L} + {}^N\boldsymbol{\alpha}^C \times (-L\hat{\mathbf{c}}_3) + {}^N\boldsymbol{\omega}^C \times {}^N\boldsymbol{\omega}^C \times (-L\hat{\mathbf{c}}_3) = \dot{u}_1\hat{\mathbf{n}}_3 + \dot{u}_3\hat{\mathbf{c}}_2 \times L\hat{\mathbf{c}}_3 - u_3\hat{\mathbf{c}}_2 \times Lu_3\hat{\mathbf{c}}_1$$
$$= \dot{u}_1\hat{\mathbf{n}}_3 + L(\dot{u}_3\hat{\mathbf{c}}_1 + u_3{}^2\hat{\mathbf{c}}_3) \tag{16}$$

Kane's dynamical equations of motion[16] for the three-particle system are given by

$$^N\mathbf{v}_r^{P_L} \cdot (\mathbf{F}_L - m_L{}^N\mathbf{a}^{P_L}) + {}^N\mathbf{v}_r^{P_B} \cdot (\mathbf{F}_B - m_C{}^N\mathbf{a}^{P_B}) + {}^N\mathbf{v}_r^{P_C} \cdot (\mathbf{F}_C - m_C{}^N\mathbf{a}^{P_C}) = 0 \qquad (r = 1, 2, 3) \tag{17}$$

For $r = 1$, we obtain

$$\hat{\mathbf{n}}_3 \cdot (\mathbf{F}_L - m_L\dot{u}_1\hat{\mathbf{n}}_3) + \hat{\mathbf{n}}_3 \cdot \{\mathbf{F}_B - m_C[\dot{u}_1\hat{\mathbf{n}}_3 + L(\dot{u}_2\hat{\mathbf{b}}_1 + u_2{}^2\hat{\mathbf{b}}_3)]\} + \hat{\mathbf{n}}_3 \cdot \{\mathbf{F}_C - m_C[\dot{u}_1\hat{\mathbf{n}}_3 + L(\dot{u}_3\hat{\mathbf{c}}_1 + u_3{}^2\hat{\mathbf{c}}_3)]\} = 0 \tag{18}$$

or

$$(m_L + 2m_C)\dot{u}_1 + m_C L(\sin\theta_1\dot{u}_2 + \sin\theta_2\dot{u}_3) = \hat{\mathbf{n}}_3 \cdot (\mathbf{F}_L + \mathbf{F}_B + \mathbf{F}_C) - m_C L(\cos\theta_1 u_2{}^2 + \cos\theta_2 u_3{}^2) \tag{19}$$

This equation of motion involves dynamic coupling between the payload translation and the rotational motion of both rigid links. For $r = 2$,

$$L\hat{\mathbf{b}}_1 \cdot \{\mathbf{F}_B - m_C[\dot{u}_1\hat{\mathbf{n}}_3 + L(\dot{u}_2\hat{\mathbf{b}}_1 + u_2{}^2\hat{\mathbf{b}}_3)]\} = L\hat{\mathbf{b}}_1 \cdot \mathbf{F}_B - m_C L(\sin\theta_1\dot{u}_1 + L\dot{u}_2) = 0 \tag{20}$$

or

$$m_C L\sin\theta_1\dot{u}_1 + m_C L^2\dot{u}_2 = L\hat{\mathbf{b}}_1 \cdot \mathbf{F}_B \tag{21}$$

Here, dynamic coupling exists between the payload translation and the rotational motion of the link attached to P_B. Finally for $r = 3$,

$$L\hat{\mathbf{c}}_1 \cdot \{\mathbf{F}_C - m_C[\dot{u}_1\hat{\mathbf{n}}_3 + L(\dot{u}_3\hat{\mathbf{c}}_1 + u_3{}^2\hat{\mathbf{c}}_3)]\} = L\hat{\mathbf{c}}_1 \cdot \mathbf{F}_C - m_C L(\sin\theta_2\dot{u}_1 + L\dot{u}_3) = 0 \tag{22}$$

or

$$m_C L\sin\theta_2\dot{u}_1 + m_C L^2\dot{u}_3 = L\hat{\mathbf{c}}_1 \cdot \mathbf{F}_C \tag{23}$$

In this case, dynamic coupling exists between the payload translation and the rotational motion of the link attached to P_C. Equation (21) is essentially the same as (23). Therefore, symmetric motion of the parachutes occurs when the magnitude of the normal force $\hat{\mathbf{b}}_1 \cdot \mathbf{F}_B$ applied to P_B is identical to the magnitude of the normal force $\hat{\mathbf{c}}_1 \cdot \mathbf{F}_C$ applied to P_C, the initial values of θ_1 and θ_2 are identical, and the initial values of $u_2 = \dot{\theta}_1$ and $u_3 = \dot{\theta}_2$ are identical. The equations of motion can be written in matrix form,

$$\begin{bmatrix} m_L + 2m_C & m_C L\sin\theta_1 & m_C L\sin\theta_2 \\ m_C L\sin\theta_1 & m_C L^2 & 0 \\ m_C L\sin\theta_2 & 0 & m_C L^2 \end{bmatrix} \begin{Bmatrix} \dot{u}_1 \\ \dot{u}_2 \\ \dot{u}_3 \end{Bmatrix} = \begin{Bmatrix} \hat{\mathbf{n}}_3 \cdot (\mathbf{F}_L + \mathbf{F}_B + \mathbf{F}_C) - m_C L(\cos\theta_1 u_2{}^2 + \cos\theta_2 u_3{}^2) \\ L\hat{\mathbf{b}}_1 \cdot \mathbf{F}_B \\ L\hat{\mathbf{c}}_1 \cdot \mathbf{F}_C \end{Bmatrix} \tag{24}$$

The mass matrix is symmetric, as expected. One can, of course, divide the second and third equations by L.

According to Ref. [3], the contribution of aerodynamic forces to $\mathbf{F}_L$ is ignored, and the force can be expressed as

$$\mathbf{F}_L = m_L g\hat{\mathbf{n}}_3 = W_L\hat{\mathbf{n}}_3 \tag{25}$$

The resultant external force applied to P_B is given by

$$\mathbf{F}_B = q_\infty S_{\text{ref}}[-(C_N)_{\text{tot}}\hat{\mathbf{b}}_1 - C_A\hat{\mathbf{b}}_3] + W_C\hat{\mathbf{n}}_3 \tag{26}$$

where W_C is the dry weight of a single parachute; the weight of the air trapped in the canopy is ignored because the gravitational force exerted on that air is assumed to be counteracted by buoyancy effects from the ambient atmosphere. The total normal force coefficient $(C_N)_{\text{tot}}$ is the sum of the free-stream normal force coefficient $(C_N)_{\text{fs}}$ and the normal force coefficient due to parachute proximity effects, $(C_N)_{\text{prox}}$,

$$(C_N)_{\text{tot}} = (C_N)_{\text{fs}} + (C_N)_{\text{prox}} \tag{27}$$

As shown in Fig. 1 and Eq. (6), $(C_N)_{\text{fs}}$ is generally a nonlinear function of α. In general, it is also a function of $\dot{\alpha}$. For this analysis it is assumed that the parachutes are oscillating about some trimmed α. Assuming small angles, $\theta' \approx \alpha'$, where θ' and α' are deviations about the trimmed θ and α respectively, and C_N varies

linearly with α. $(C_N)_{\text{prox}}$ is a function of D_{prox}, the distance between the parachute centers, and V_{prox}, the time derivative of D_{prox}. Proximity distance can be expressed as $D_{\text{prox}} = 2L\sin\theta$, and its time derivative is thus $V_{\text{prox}} = 2L\cos\theta\dot{\theta}$. The derivatives of the normal force coefficients have a relationship similar to Eq. (27).

$$(C_{N_\alpha})_{\text{tot}} = (C_{N_\alpha})_{\text{fs}} + (C_{N_\alpha})_{\text{prox}} \tag{28}$$

The resultant external force applied to P_C is given by

$$\mathbf{F}_C = q_\infty S_{\text{ref}}[-(C_N)_{\text{tot}}\hat{\mathbf{c}}_1 - C_A\hat{\mathbf{c}}_3] + W_C\hat{\mathbf{n}}_3 \tag{29}$$

The dynamical equations of motion (Eq. 24) can be solved numerically to obtain insights into the scissors motion as shown in Fig. 4. System parameters are listed in Table 5. A representative value of $(C_{N_\alpha})_{\text{tot}} = 0.225$ rad^{-1} is used and zero damping due to $\dot{\alpha}$ and V_{prox} is assumed. The three-particle system is translating in the direction of $\hat{\mathbf{n}}_3$ while P_B and P_C oscillate symmetrically about their respective trimmed α (or θ). It is most interesting to note that as the parachutes fly outwards away from the vertical axis, the descent rate $u_1 = w_L$ of P_L decreases in magnitude. Conversely, as the parachutes move inwards, w_L increases in magnitude. This phenomenon is a result of the dynamic coupling present in the system.

Table 5. System Parameters.

parameter	value	units
S_{ref} (single parachute)	10563	ft^2
L	235	ft
Capsule Weight, W_L	21906	lb$_{\text{f}}$
Dry Weight of One Parachute, W_C	327	lb$_{\text{f}}$
Total Mass of One Parachutes, (dry and entrapped air), m_C	307	slugs

If the dynamic coupling in Eqs. (24) is ignored (valid approximation since contribution of $\dot{u}_1$ to $\dot{u}_2$ is small), damping is neglected, and θ_1 is assumed to remain small, the second of Eqs. (24) describes an undamped harmonic oscillation:
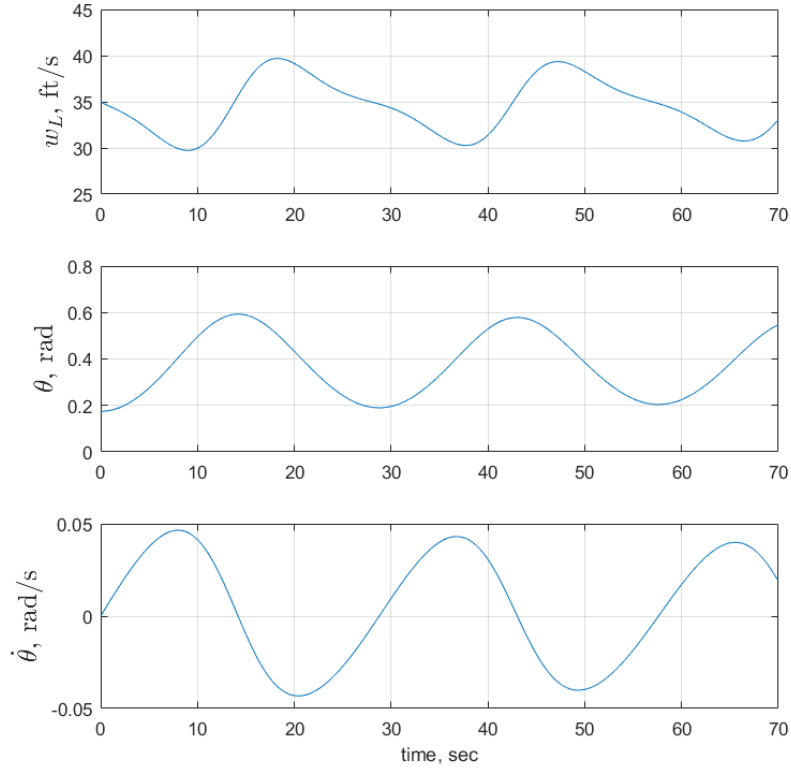
$$\dot{u}_2 = \ddot{\theta}_1 \approx \frac{W_C - q_\infty S_{\text{ref}}(C_{N_\alpha})_{\text{tot}}}{m_C L}\theta_1 \tag{30}$$

The period associated with the scissors motion, T, is found to be inversely proportional to $(C_{N_\alpha})_{\text{tot}}$

$$T = 2\pi\sqrt{\frac{m_C L}{q_\infty S_{\text{ref}}(C_{N_\alpha})_{\text{tot}} - W_C}} \tag{31}$$

$(C_{N_\alpha})_{\text{tot}}$ can be expressed as a function of T and key system parameters:

$$(C_{N_\alpha})_{\text{tot}} = \frac{1}{q_\infty S_{\text{ref}}}\left(\frac{4\pi^2 m_C L}{T^2} + W_C\right) \tag{32}$$

American Institute of Aeronautics and Astronautics

Figure 4. Scissors Mode Simulation Results

The scissors motion observed during the CDT 3-02 and 3-08 flights is shown in Fig. 5. The motion is approximately planar in nature. The red and blue curves indicate the paths traced out by the parachutes relative to the capsule during one cycle of the flyout motion. The observed period of oscillation from both flights is roughly 12 seconds. From Eq. (32), a value of $(C_{N_\alpha})_{\text{tot}} = 1.9$ rad^{-1} can be determined. A value of 0.4 rad^{-1} was determined for $(C_{N_\alpha})_{\text{fs}}$ from the pendulum motion analysis shown in Table 1. This suggests that $(C_{N_\alpha})_{\text{prox}}$ should be on the order of 1.5 rad^{-1}.
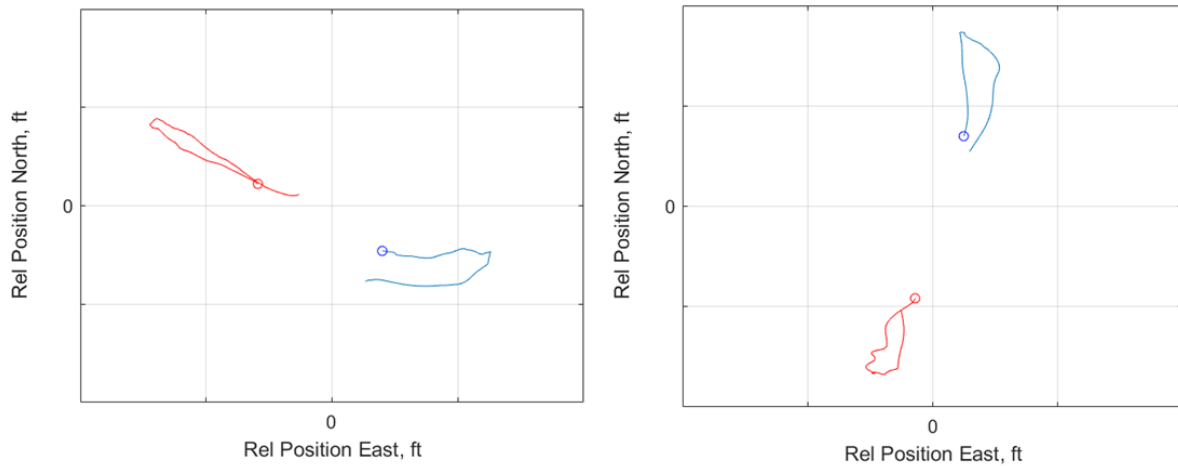
Figure 5. Scissors Motion from Flight Data. CDT 3-02 (left), CDT 3-08 (right)

American Institute of Aeronautics and Astronautics

Figure 6 shows derived measurements taken during the CDT 3-02 flight of the total normal force coefficient, $(C_N)_{\text{tot}}$ resolved along the proximity axis with the corresponding proximity distance, D_{prox}, for each parachute. D_{prox} is normalized by the nominal diameter of the parachutes, 116 ft. The data appears to be fairly linear for $\zeta_1 \leq D_{\text{prox}} \leq \zeta_2$ and flattens out for $D_{\text{prox}} > \zeta_2$. The red line indicates a least-squares linear fit. It is apparent that $(C_N)_{\text{tot}}$ has an equilibrium at D_{prox} of ζ_1 (or $\theta_o = \theta_1 = \theta_2 = \alpha$ rad). The slope of the least-squares fit is approximately 1.9 rad^{-1}, which is consistent with the analysis of the scissors motion in isolation as described in the previous paragraph. Same exercises were performed with plots not presented here for the CDT 3-08, CDT 3-11, and CDT 3-12 flights, all of which yielded similar results.
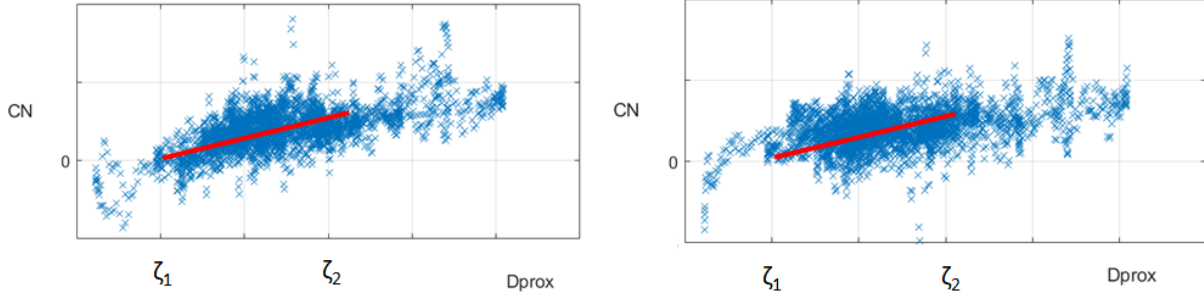

Figure 6. $(C_N)_{\text{prox}}$ **from CDT 3-02. Parachute #1 (left), Parachute #2 (right)**

IV. Maypole Mode

Maypole motion described in Ref. [2] consists of two parachutes orbiting about the vertical axis. Ref. [12] refer to it as the spiral motion. A simplified model used to study maypole motion is illustrated in Fig. 7. The three particles P_L, P_B, and P_C are the same as those described in Sec. III; in the present model, however, all three are assumed to be fixed in a rigid body B. A right-handed set of mutually perpendicular unit vectors $\hat{\mathbf{b}}_1$, $\hat{\mathbf{b}}_2$, and $\hat{\mathbf{b}}_3$ is fixed in B and directed as shown in Fig. 7. $\hat{\mathbf{b}}_2$ is normal to the plane containing P_L, P_B, and P_C. $\hat{\mathbf{b}}_3$ is parallel to an axis of symmetry of B, which is therefore a central principal axis of inertia of B. A dextral set of mutually perpendicular unit vectors $\hat{\mathbf{n}}_1$, $\hat{\mathbf{n}}_2$, and $\hat{\mathbf{n}}_3$ is fixed in a Newtonian reference frame N. $\hat{\mathbf{n}}_1$ is horizontal, $\hat{\mathbf{n}}_2$ is directed out of the page, and $\hat{\mathbf{n}}_3$ is vertical, directed downward. B moves in N such that $\hat{\mathbf{b}}_3 = \hat{\mathbf{n}}_3$ at all times. Moreover, the velocity in N of every point on the axis of symmetry of B has the same constant magnitude and the same direction as $\hat{\mathbf{n}}_3$. For example, P_L lies on the axis of symmetry, so the velocity of P_L in N can be written as

$$^N\mathbf{v}^{P_L} = V_3\hat{\mathbf{n}}_3 \qquad (33)$$

where V_3 is a constant. Hence, the acceleration in N of P_L and every point on the axis of symmetry is zero,

$$^N\mathbf{a}^{P_L} = \mathbf{0} \qquad (34)$$

The mass center of B, denoted by $B^\star$, lies on the axis of symmetry and therefore has an acceleration in N equal to zero. Based on first principles, this requires that the resultant of all external forces applied to B is equal to zero. The angular velocity $^N\boldsymbol{\omega}^B$ of B in N that characterizes maypole motion is parallel to a central principal axis of inertia of B.

$$^N\boldsymbol{\omega}^B = \Omega\hat{\mathbf{b}}_3 = \Omega\hat{\mathbf{n}}_3 \qquad (35)$$

where Ω is a constant. Thus, it can be seen that the angular acceleration $^N\boldsymbol{\alpha}^B$ of B in N is zero,

$$^N\boldsymbol{\alpha}^B = \mathbf{0} \qquad (36)$$

Euler's rotational equations of motion are satisfied by Eqs. (35) and (36) only if the resultant moment about $B^\star$ of all external forces applied to B is equal to zero.

Two additional sets of dextral, mutually perpendicular unit vectors are introduced for convenience in conducting kinematic analysis and expressing the forces applied to B. Both sets of unit vectors are fixed in B. The first set contains $\hat{\mathbf{e}}_1$, $\hat{\mathbf{e}}_2$, and $\hat{\mathbf{e}}_3$, whereas the second set contains $\hat{\mathbf{f}}_1$, $\hat{\mathbf{f}}_2$, and $\hat{\mathbf{f}}_3$. The relationships of

American Institute of Aeronautics and Astronautics

each set of unit vectors to $\hat{\mathbf{b}}_1$, $\hat{\mathbf{b}}_2$, and $\hat{\mathbf{b}}_3$ are given in Tables 6 and 7, where the constant angle Φ is shown in Fig. 7.

P_L, P_B, and P_C are all fixed in B; therefore, the velocities in N of P_B and P_C can be expressed in terms of ${}^N\mathbf{v}^{P_L}$.

$$
{}^N\mathbf{v}^{P_B} = {}^N\mathbf{v}^{P_L} + {}^N\boldsymbol{\omega}^B \times (-L\hat{\mathbf{e}}_3) = V_3\hat{\mathbf{n}}_3 - \Omega\hat{\mathbf{b}}_3 \times L(-\sin\Phi\hat{\mathbf{b}}_1 + \cos\Phi\hat{\mathbf{b}}_3) = V_3\hat{\mathbf{n}}_3 + \Omega L\sin\Phi\hat{\mathbf{b}}_2 \quad (37)
$$

$$
{}^N\mathbf{v}^{P_C} = {}^N\mathbf{v}^{P_L} + {}^N\boldsymbol{\omega}^B \times (-L\hat{\mathbf{f}}_3) = V_3\hat{\mathbf{n}}_3 - \Omega\hat{\mathbf{b}}_3 \times L(\sin\Phi\hat{\mathbf{b}}_1 + \cos\Phi\hat{\mathbf{b}}_3) = V_3\hat{\mathbf{n}}_3 - \Omega L\sin\Phi\hat{\mathbf{b}}_2 \quad (38)
$$

The accelerations in N of P_B and P_C are then determined to be

$$
{}^N\mathbf{a}^{P_B} = \mathbf{0} + \Omega L\sin\Phi\,{}^N\boldsymbol{\omega}^B \times \hat{\mathbf{b}}_2 = \Omega L\sin\Phi\,\Omega\hat{\mathbf{b}}_3 \times \hat{\mathbf{b}}_2 = -R\Omega^2\hat{\mathbf{b}}_1 \quad (39)
$$

$$
{}^N\mathbf{a}^{P_C} = \mathbf{0} - \Omega L\sin\Phi\,{}^N\boldsymbol{\omega}^B \times \hat{\mathbf{b}}_2 = -\Omega L\sin\Phi\,\Omega\hat{\mathbf{b}}_3 \times \hat{\mathbf{b}}_2 = R\Omega^2\hat{\mathbf{b}}_1 \quad (40)
$$

where $R = L\sin\Phi$, as indicated in Fig. 7.

The resultants of the external forces acting on P_L, P_B, and P_C are once again denoted by $\mathbf{F}_L$, $\mathbf{F}_B$, and $\mathbf{F}_C$, respectively. As in Sec. III, $\mathbf{F}_L$ is expressed as

$$
\mathbf{F}_L = m_L g\hat{\mathbf{n}}_3 = W_L\hat{\mathbf{n}}_3 \quad (41)
$$

The resultant external force applied to P_B is in general given by

$$
\mathbf{F}_B = q_\infty S_{\mathrm{ref}}[-(C_N)_{\mathrm{tot}}\hat{\mathbf{e}}_1 + C_Y\hat{\mathbf{e}}_2 - C_A\hat{\mathbf{e}}_3] + W_C\hat{\mathbf{n}}_3 \quad (42)
$$

where W_C is the dry weight of a single parachute. $(C_N)_{\mathrm{tot}}$ can in this case be expressed as in Eq. (27). In addition, it is assumed that $\Phi = \alpha$ and the parachutes are in static equilibrium with constant flyout angles and at some trimmed angle of attack, α_{trim}, while performing the maypole motion. The resultant external force applied to P_C is similar to $\mathbf{F}_B$.

$$
\mathbf{F}_C = q_\infty S_{\mathrm{ref}}[-(C_N)_{\mathrm{tot}}\hat{\mathbf{f}}_1 + C_Y\hat{\mathbf{f}}_2 - C_A\hat{\mathbf{f}}_3] + W_C\hat{\mathbf{n}}_3 \quad (43)
$$

However, the side forces associated with C_Y would yield a nonzero moment about $B^\star$ that is parallel to $\hat{\mathbf{b}}_3$. Hence, maypole motion requires
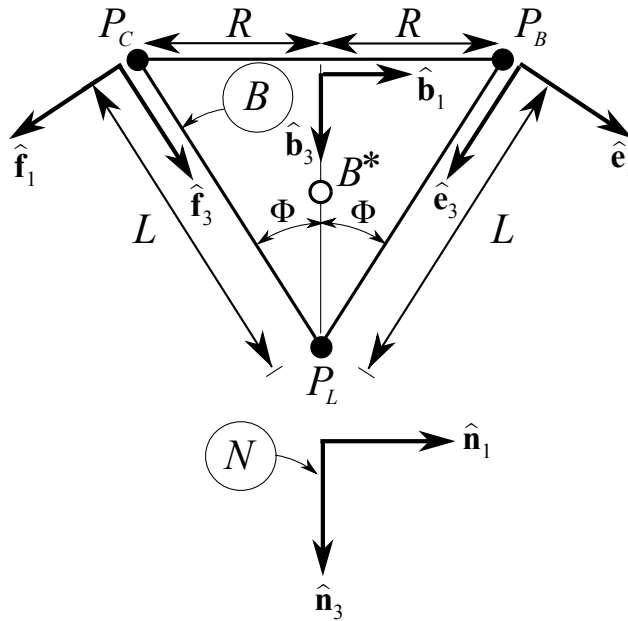
$$
C_Y = 0 \quad (44)
$$

Figure 7. Maypole Mode Model

American Institute of Aeronautics and Astronautics

Table 6. Direction Cosines, $\hat{\mathbf{b}}_r \cdot \hat{\mathbf{e}}_s$.

	$\hat{\mathbf{e}}_1$	$\hat{\mathbf{e}}_2$	$\hat{\mathbf{e}}_3$
$\hat{\mathbf{b}}_1$	$\cos\Phi$	0	$-\sin\Phi$
$\hat{\mathbf{b}}_2$	0	1	0
$\hat{\mathbf{b}}_3$	$\sin\Phi$	0	$\cos\Phi$

Table 7. Direction Cosines, $\hat{\mathbf{b}}_r \cdot \hat{\mathbf{f}}_s$.

	$\hat{\mathbf{f}}_1$	$\hat{\mathbf{f}}_2$	$\hat{\mathbf{f}}_3$
$\hat{\mathbf{b}}_1$	$-\cos\Phi$	0	$\sin\Phi$
$\hat{\mathbf{b}}_2$	0	-1	0
$\hat{\mathbf{b}}_3$	$\sin\Phi$	0	$\cos\Phi$

Because P_L and P_B are connected by a rigid link, each exerts a force on the other. The force exerted by P_L on P_B can be expressed as $T\hat{\mathbf{e}}_3$. This internal force must be accounted for when applying Newton's second law to P_B; however, forming dot products with $\hat{\mathbf{e}}_1$ will eliminate T. That is,

$$(\mathbf{F}_B + T\hat{\mathbf{e}}_3) \cdot \hat{\mathbf{e}}_1 = \mathbf{F}_B \cdot \hat{\mathbf{e}}_1 = m_C \,^N\mathbf{a}^{P_B} \cdot \hat{\mathbf{e}}_1 \tag{45}$$

Upon substitution from Eqs. (39) and (42), we have

$$\begin{aligned}
\{q_\infty S_{\text{ref}}[-(C_N)_{\text{tot}}\hat{\mathbf{e}}_1 - C_A\hat{\mathbf{e}}_3] + W_C\hat{\mathbf{n}}_3\} \cdot \hat{\mathbf{e}}_1 &= -q_\infty S_{\text{ref}}(C_N)_{\text{tot}} + W_C \sin\Phi \\
&= -m_C R\Omega^2 \hat{\mathbf{b}}_1 \cdot \hat{\mathbf{e}}_1 \\
&= -m_C R\Omega^2 \cos\Phi
\end{aligned} \tag{46}$$

This relationship can be solved for $(C_N)_{\text{tot}}$,

$$(C_N)_{\text{tot}} = \frac{m_C R\Omega^2 \cos\Phi + W_C \sin\Phi}{q_\infty S_{\text{ref}}} \tag{47}$$

Thus, the aerodynamic normal force is seen to be directly proportional to the magnitude of the centripetal acceleration of P_B (or P_C). One can also conclude that the radius and period of the maypole mode is dependent on the value of $(C_N)_{\text{tot}}$ at α_{trim}. For a given orbital radius R, the orbital angular rate is given by

$$\Omega = \sqrt{\frac{q_\infty S_{\text{ref}}(C_N)_{\text{tot}} - W_C \sin\Phi}{m_C R \cos\Phi}} \tag{48}$$

The orbital period of maypole motion is thus seen to be inversely proportional to $(C_N)_{\text{tot}}$. This conclusion appears to contradict the findings in Ref. [12] which suggests that the orbital period increases with C_N. However, the authors of Ref. [12] state that those results are only applicable to a narrow range of initial conditions. Hence, that may explain the discrepancy. Finally, by appealing to the fact that the resultant external force applied to B must be $\mathbf{0}$ in order for maypole motion to take place, a relationship between $(C_N)_{\text{tot}}$ and C_A can be obtained. The resultant is given by

$$\mathbf{F}_B + \mathbf{F}_C + \mathbf{F}_L = q_\infty S_{\text{ref}}[-(C_N)_{\text{tot}}(\hat{\mathbf{e}}_1 + \hat{\mathbf{f}}_1) - C_A(\hat{\mathbf{e}}_3 + \hat{\mathbf{f}}_3)] + (2W_C + W_L)\hat{\mathbf{n}}_3 = \mathbf{0} \tag{49}$$

Hence,

$$\begin{aligned}
(\mathbf{F}_B + \mathbf{F}_C + \mathbf{F}_L) \cdot \hat{\mathbf{b}}_3 &= \{q_\infty S_{\text{ref}}[-(C_N)_{\text{tot}}(\hat{\mathbf{e}}_1 + \hat{\mathbf{f}}_1) - C_A(\hat{\mathbf{e}}_3 + \hat{\mathbf{f}}_3)] + (2W_C + W_L)\hat{\mathbf{n}}_3\} \cdot \hat{\mathbf{b}}_3 \\
&= -q_\infty S_{\text{ref}}(2(C_N)_{\text{tot}} \sin\Phi + 2C_A \cos\Phi) + 2W_C + W_L \\
&= 0
\end{aligned} \tag{50}$$

or

$$(C_N)_{\text{tot}} = \frac{2W_C + m_L g - 2q_\infty S_{\text{ref}} C_A \cos\Phi}{2q_\infty S_{\text{ref}} \sin\Phi} \tag{51}$$

According to Ref. [2], the CDT 3-02 flight exhibited one full period of the maypole motion, as illustrated in Fig. 8. The motion is approximately circular in nature and lasted for about 50 seconds. The red and blue curves indicate the paths traced out by the parachutes relative to the capsule during the maypole motion.
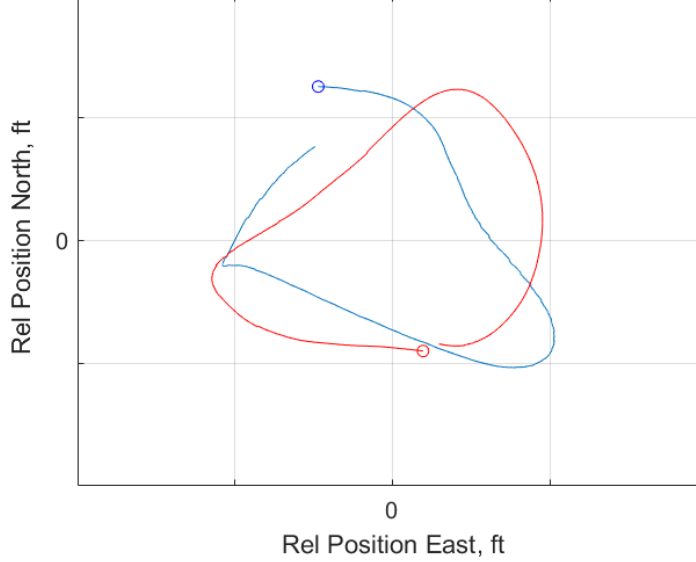
Figure 8. Maypole Motion from Flight Data

The analysis discussed in this section is based on the assumption that during the maypole motion the parachutes orbit around the vertical axis of symmetry in a perfect circle with a constant angular speed. To analyze the flight data, the line integrals of the paths traced out by the parachutes during the maypole motion were computed. This resulted in an equivalent circle with a radius of 60 ft or a constant flyout angle (or α_{trim}) of 0.26 rad. This is consistent with the observation from Ref. [12] that the interference aerodynamic forces cause the unstable parachutes to seek a trim angle of attack greater than the freestream trim α (0.23 rad shown in Table 1). Using Eq. (47), the normal force coefficient required to maintain the maypole motion is determined to be approximately 0.03. This result is consistent with the analysis from Sec. III which suggests that the scissors and maypole modes are dominated by proximity aerodynamics.

V.   Breathing Mode

Parachutes are made out of flexible materials and are inherently non-rigid objects. As they deform during flight, the projected reference area S_{proj} changes and affects the axial motion of the system. Ref. [2] describes this axial oscillatory behavior as the "breathing mode." CDT 3-02 flight test data showed that during the breathing mode as the canopies contracted from the nominal reference area, V_{down} increased; conversely, as the canopies increased from the nominal reference area, V_{down} decreased. This oscillatory behavior occurred with a period of 7 seconds.

The underlying dynamics of the breathing mode is straightforward and can be represented by Eqs. (52)–(54). The parameter η is used to approximate the deformation of the chute away from its nominal projected area. The oscillatory deformation behavior can be represented by a second-order harmonic oscillator. The natural frequency ω_n is dependent on many parameters such as the parachute material properties, porosity, natural environments, etc.

$$\ddot{\eta} + d\dot{\eta} + \omega_n^2 \eta = 0 \tag{52}$$

The axial force coefficient consists of a baseline term and a term dependent on η:

$$C_A = C_{A_0} + C_{A_\eta} \eta \tag{53}$$

The equation of motion in the down direction is as follows:

$$(m_L + 2m_{C,\text{dry}})\dot{w} = S_{\text{ref}}\rho w^2 C_A + (m_L + 2m_{C,\text{dry}})g \tag{54}$$

Figure 9 shows simulation results for the breathing mode with the system having a nominal V_{down} of approximately 34 ft/s. ω_n is scaled such that the period of oscillation is around 7 seconds to match the flight data.

American Institute of Aeronautics and Astronautics

$\eta = 0$ represents the nominal S_{proj}, while $\eta = \pm 1$ represents S_{proj} at its maximum and minimum derivations from the nominal. It is apparent that as η approaches 1, V_{down} approaches its minimum value of 32 ft/s and as η approaches -1, V_{down} approaches its maximum value of 35.2 ft/s. Furthermore, η has a slight phase lead on V_{down} as one would expect.
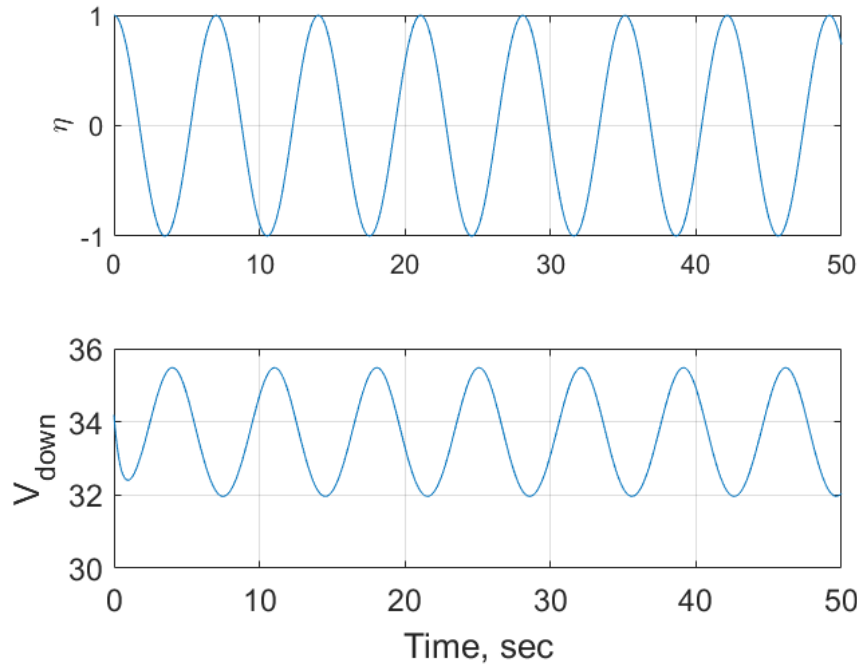

Figure 9. Breathing Mode Simulation Results

VI. Conclusion

The overall motion of a system containing two parachutes and a capsule is extremely complicated with nonlinearities and flexibility effects. It is usually difficult to obtain insight into the fundamental dynamics of the system by examining results from a multi-body simulation based on nonlinear equations of motion. In the current work, the dynamics of the scissors, maypole, breathing, and pendulum modes observed during various drop tests is studied on an individual basis by using a simplified dynamics model for each mode. Analysis of the flight data shows that the scissors and maypole modes are largely dominated by proximity aerodynamics. The separate studies of each mode produce compatible results and provide a better understanding of the behavior of the complex multi-body system.

VII. Acknowledgements

References

[1] Ray, E. S., and Machín, R. A., "Pendulum Motion in Main Parachute Clusters," No. 2015-2138, AIAA, 2015.

[2] Ali, Y., Sommer, B., Troung, T., Anderson, B., and Madsen, C., "Orion Multi-Purpose Crew Vehicle Solving and Mitigating the Two Main Cluster Pendulum Problem," No. 2017-4056, *24rd Aerodynamic Decelerator Conference*, AIAA, 2017.

[3]White, F. M., and Wolf, D. F., "A Theory of Three-Dimensional Parachute Dynamic Stability," *Journal of Aircraft*, Vol. 5, No. 1, 1968, pp. 86–92.

[4]Ginn, J. M., Clark, I. G., and Braun, R. D., "Parachute Dynamic Stability and the Effects of Apparent Inertia," No. 2014-2390, AIAA, 2014.

[5]Eaton, J. A., "Added Mass and the Dynamic Stability of Parachutes," *Journal of Aircraft*, Vol. 19, No. 5, 1982, pp. 414–416.

[6]Knacke, T. W., *Parachute Recovery Systems Design Manual*, Para Publications, Santa Barbara, 1991.

[7]Greathouse, J., and Schwing, A., "Study of Geometric Porosity and Drag using Computational Fluid Dynamics for Rigid Parachute Shapes," No. 2015-2131, *23rd Aerodynamic Decelerator Conference*, AIAA, 2015.

[8]Roithmayr, C. M., Beaty, J., Pei, J., Barton, R. L., and Matz, D. A., "Linear Analysis of Two-Parachute System Undergoing Pendulum Motion," submitted, 25th Aerodynamic Decelerator Conference, AIAA, 2019.

[9]Pei, J., "Nonlinear Analysis of a Two-Parachute Cluster System Undergoing Pendulum Motion," submitted, 25th Aerodynamic Decelerator Conference, AIAA, 2019.

[10]Murri, D., Morelli, E., Pei, J., Roithmayr, C., Matz, D., Barton, R., and Mendenhall, M., "Application of System Identification to Parachute Modeling," NASA Engineering and Safety Center Technical Assessment Report, May 23, 2019

[11]Etkins, B., *Dynamics of Atmospheric Flight*, Dover Publications, Mineola, NY. 2000.

[12]Wolf, D., and Heindel, K., "A Steady Rotation Motion for a Cluster of Parachutes," No. 2005-1629, AIAA, 2005.

[13]Pamadi, B. N., *Performance, Stability, Dynamics, and Control of Airplanes*, 3rd Ed, AIAA, 2015, pp. 427-428.

[14]Morelli, E. A., and Klein, V., *Aircraft System Identification, Theory and Practice*, Sunflyte Enterprises, Williamsburg, VA. 2016.

[15]Morelli, E. A., "System IDentification Programs for AirCraft (SIDPAC)," http://software.nasa.gov.

[16]Kane, T. R., and Levinson, D. A., *Dynamics: Theory and Applications*, McGraw-Hill, New York, 1985, pp. 45–50, 158–159.